Available online at www.sciencedirect.com
ScienceDirect
Journal of Power Sources 175 (2008) 517–525
JOURNAL OF POWER SOURCES
www.elsevier.com/locate/jpowsour

Layered lithium cobalt nitrides: A new class of lithium intercalation compounds

J.B. Ducros [a], S. Bach [a,*], J.P. Pereira-Ramos [a], P. Willmann [b]

[a] *Institut de Chimie et des Matériaux Paris Est, GESMAT, UMR CNRS 7182, 2 rue Henri-Dunant, 94320 Thiais, France*
[b] *Centre National d'Etudes Spatiales, 118 avenue Edouard Belin, 31401 Toulouse Cedex 9, France*

Received 5 July 2007; received in revised form 23 August 2007; accepted 16 September 2007
Available online 22 September 2007

Abstract

Lithium cobalt nitrides $Li_{3-2x}Co_xN$ ($0.1 \leq x \leq 0.44$) have been prepared and investigated as negative electrode in the 1/0.02 V potential window. The evolution of the unit cell parameters and unit cell volume with the Co content show a solid solution behaviour. Whatever the Co content, all these nitrides are electroactive with a single step around 0.6 V/0.7 V for the discharge and charge processes, respectively. The electrochemical behaviour observed is typical of a Li intercalation compound and involves the Co^{2+}/Co^{+} redox couple in the interlayer plane combined with the reversible accommodation of Li^+ ions in the cation vacancies located in Li_2N^- layers. XRD experiments performed after discharge, charge and cycling tests clearly indicate the hexagonal layered structure of the host lattice is maintained. This intercalation process explains the excellent capacity retention found after 50 cycles. A specific capacity of 180 mAh g^{-1} at *C*/20 and 130 mAh g^{-1} at *C*/5 rate (100 mA cm^{-2}) is achieved for $Li_{2.23}Co_{0.39}N$. ac impedance measurements have allowed to characterize the kinetics of the reaction.

Keywords: Lithium cobalt nitrides; Lithium insertion; Negative electrode; Lithium batteries

1. Introduction

The explosive demand for portable devices, such as portable telephones and notebook type computers has increased the importance of Li-ion battery [1]. This system has the highest specific energy among the available battery systems and is based on a high voltage cathode working at 4.2 V and an anode that works at around 0.2–0.1 V versus Li/Li^+. The commercialized lithium-ion batteries use graphite as negative electrode, but it suffers of a low capacity, i.e., 372 mAh g^{-1}. Therefore various carbonaceous compounds have also been investigated as possible negative electrodes [2,3]. In recent years, a great effort has been made to find alternative anode materials to replace graphite in Li-ion batteries. Possible improvements have been proposed with the use of other candidates such as some alloys, i.e., LiAl, LiSn [4–6], tin oxides leading to the formation of Li_xSn alloys [7–10] but the dramatic volumetric changes responsible of the capacity loss upon cycling has never been solved as yet. A new class of negative materials is now receiving considerable attention such as cobalt, nickel, iron and manganese oxides working in the 3–0.01 V potential range through conversion reactions leading to sustained high reversible capacities [11,12].

Another group of attractive negative materials is formed by the transition metal pnictides compounds M–Pn with Pn = P [13–16], Sb [17], N [18–25]. In the case of the transition metal nitrides, the Li_3FeN_2 and Li_7MnN_4 compounds exhibit capacities in the range 150–250 mAh g^{-1} at 1.2/1.1 V [24,25]. More interesting properties have been evidenced with the lithium cobalt nitrides with the chemical composition $Li_{3-x}Co_xN$ ($0 \leq x \leq 0.6$) [18–22], these nitride solid solutions exhibiting a layered structure characterized by an hexagonal symmetry (P_6/mmm). Most of the papers in this area focus on $Li_{2.6}Co_{0.4}N$ which seems to be the most promising compound. However, contradictory capacity values are reported for that anode material with a remarkable stable capacity of 760 mAh g^{-1} recovered after 50 cycles performed in the 1.4/0 V range [18,19] which is twice that achieved by another team [20,21].

In all cases the authors systematically investigated these materials using first a charge up to 1.4 V involving an irreversible structural change which is not well understood as yet.

* Corresponding author. Tel.: +33 1 4978 1200; fax: +33 1 4978 1323.
E-mail address: Bach@glvt-cnrs.fr (S. Bach).

0378-7753/$ – see front matter © 2007 Elsevier B.V. All rights reserved.
doi:10.1016/j.jpowsour.2007.09.052

The lack of data on the discharge–charge behaviour of the lithium cobalt nitrides $Li_{3-x}Co_xN$ for $x \neq 0.4$ and the contradictory results on the cycling properties of $Li_{2.6}Co_{0.4}N$ has prompted us to investigate the structural and electrochemical properties of the ternary lithium cobalt nitrides in the limited potential range 1–0.02 V with the hope of limited structural rearrangements and attractive specific capacities. This investigation of the Li–Co–N system will be done at the light of a detailed chemical and structural characterization.

2. Experimental

2.1. Chemical synthesis and structural analysis

The lithium cobalt nitride compounds were prepared using a solid state route from the reagent grade Li_3N (Alfa-Aesar 99.5%, 10 μm) and Co metal (Alfa-Aesar 99.8%, 1.6 μm). To obtain $Li_{3-x}Co_xN$ with different x values, a mixture of Li_3N and Co in a ratio R ($R = Co/Li_3N$) was first mixed and ground in agate mortar and was then pressed to get a pellet 1 cm in diameter and 5–8 mm in thickness. The pellet of about 1 g is then transferred on a tungsten foil in an alumina crucible and heat-treated at desired temperatures at 700 °C for 8 h in a nitrogen gas stream. The oven is first at 300 °C and a heating rate of 50 °C h^{-1} is used to reach 700 °C.

XRD experiments were performed on a Brucker D8 diffractometer using Cu Kα radiation ($\lambda = 1.54178$ Å). Step scan recordings were carried out by using 0.02° 2θ steps of 10 s duration. The chemical composition of the compounds was determined by elemental analysis (inductively coupled plasma-atomic emission spectroscopy: ICP-AES) with an accuracy of ±2%.

2.2. Electrochemical measurements

The electrolyte used was 1 mol L^{-1} $LiPF_6$ in ethylene carbonate (EC) and diethyl carbonate (DEC) solution (1:2, v/v). The working electrode consisted of a stainless steel grid (12 mm diameter, 0.2 mm thickness) with a geometric area of ≈1 cm^2 on which the cathode material was pressed (5 t cm^{-2}). The cathode was made of a mixture of active material (70 wt%), acetylene black or nickel powder (in order to eliminate the SEI formation) (22 wt%) and teflon as binder agent (8%). Electrochemical studies were carried out in two-electrodes cells (Swagelok® type) or three-electrodes cells. In that case, the counter electrode consisted of a lithium foil and the reference electrode consisted of a lithium wire in a separate compartment. Electrochemical measurements were made with a Mac Pile apparatus. Galvanostatic discharge–charge tests between 1 and 0.02 V versus Li/Li^+ were carried out at $C/2$, $C/5$, $C/10$ and $C/20$ rate. Impedance spectroscopy experiments were carried out in the frequency range 10^4 to 10^{-4} Hz using an EGG (PAR) potentiostat coupled with a 1255 Schlumberger Frequency Response Analyser. The excitation signal was 5 mV peak to peak. The equilibrium potential was considered to be reached when the drift in open-circuit voltage remained less than 1 mV during 5 h.

Software Carine® was used for the simulation of XRD patterns.

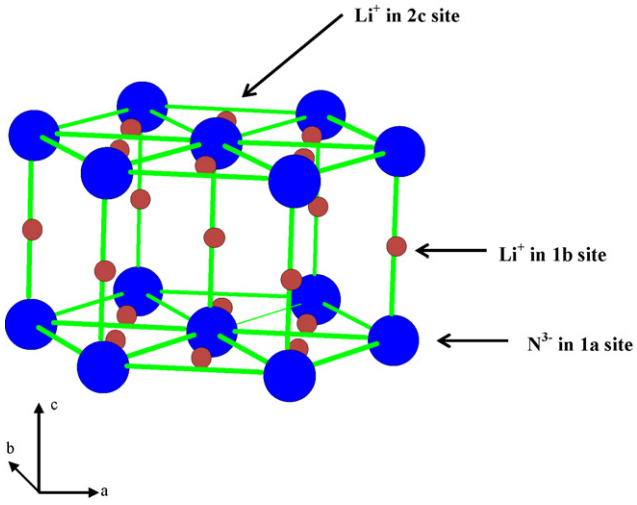

Fig. 1. Crystal structure of α-Li_3N.

3. Results and discussion

The layered compound α-Li_3N exhibits an hexagonal structure (space group P_6/mmm) illustrated in Fig. 1. This structure is characterized by the stacking of alternate layers of Li_2N^- in which the Li^+ cations and the N^{3-} anions occupy all the 2c sites and the 1a sites, respectively, and pure Li planes. In that planes, lithium ions are localized in the 1b sites.

After reaction, the pellets of the lithium cobalt nitrides corresponding to a single phase ($R \leq 0.6$) are dissolved in a 2N H_2SO_4 aqueous solution at room temperature and the amount of Li and Co moles is determined by ICP-AES measurements. Table 1 summarizes the chemical compositions for the products obtained after reaction between cobalt and lithium nitride according to the schematic reaction usually reported in literatures [18–21]: $Li_3N_{(s)} + x\ Co_{(s)} \rightarrow Li_{3-x}Co_xN$ or $Li_3N_{(s)} + xCo_{(s)} \rightarrow Li_{3-2x}Co_xN$ depending on the oxidation state of cobalt, Co(I) and Co(II), respectively. The chemical compositions drawn from literatures [20,21,26–29] are given in Table 1 for comparison. R is the experimental molar ratio of reactants Co/Li_3N used for the synthesis reaction, not the

Table 1
Chemical compositions of the products obtained after reaction between cobalt and lithium nitride, R = the experimental molar ratio of reactants (Co/Li_3N)

R	Chemical composition [this work]		Chemical composition []
	Co^I formation	Co^{II} formation	
0.1	$Li_{2.91}Co^I_{0.10}N$	$Li_{2.79}Co^{II}_{0.10}N$	$Li_{2.9}Co_{0.1}N$ [20,26]
0.2	$Li_{2.80}Co^I_{0.19}N$	$Li_{2.64}Co^{II}_{0.18}N$	$Li_{2.8}Co_{0.2}N$ [20]
			$Li_{2.7}Co_{0.3}N$ [26]
0.3	$Li_{2.70}Co^I_{0.29}N$	$Li_{2.46}Co^{II}_{0.27}N$	$Li_{2.57}$ $Co_{0.3}N$ [20]
			$Li_{2.4}Co_{0.3}N$ [21]
			$Li_{2.6}Co_{0.4}N$ [22,27–29]
			$Li_{2.42}Co_{0.4}N$ [20]
0.4	$Li_{2.63}Co^I_{0.37}N$	$Li_{2.35}Co^{II}_{0.33}N$	$Li_{2.30}Co_{0.4}N$ [21]
			$Li_{2.56}Co_{0.44}N$ [30]
			$Li_{2.23}Co_{0.39}N$ [30]
0.5	$Li_{2.55}Co^I_{0.44}N$	$Li_{2.23}Co^{II}_{0.39}N$	
0.6	$Li_{2.50}Co^I_{0.51}N$	$Li_{2.12}Co^{II}_{0.44}N$	

effective cobalt content in the lithium cobalt nitride. Indeed, the elemental analysis reveals a lithium loss (in the range 4–11%) which increases with the cobalt content. We also found a significant loss of cobalt (≈5–9%) when R exceeds 0.3. The loss of Li and Co could be explained by the formation of the corresponding nitrides and their sublimation as suggested by the silica tube attacked by nitride vapors. The determination of the nitrogen content obtained in each sample is deduced from the charge balance with the positive charge provided by the results of the chemical analysis by ICP-AES for the Li and Co elements. During the reaction, the presence of a nitrogen gas stream allows the oxidation of cobalt metal. Considering the reaction consists in a substitution reaction of Li^+ by Co^+ or Co^{2+}, two chemical compositions can be suggested for the final products. Though the oxidation state of Co has not been established [18–21], it can be assumed that Co(II) would be preferentially formed during the synthesis because (i) Co(II) and Co(III) are the most common oxidation states for Co in solid state chemistry; (ii) the ionic radius of Li^+ ion (0.4 Å) is very close to that of Co^{2+} in ionic nitrides [31]. In that case, in addition to the formation of Co(II) ions, the equation reaction must account for the substitution of Li^+ ions by Co^{2+} ions and the correlative presence of lithium vacancies, □. Therefore the synthesis reaction could be written as

$$Li_3N_{(s)} + R\,Co_{(s)} \xrightarrow{N_2} Li_{3-2x}Co^{II}_x\square_xN_{(s)} \quad \text{with } x \le R$$

In Fig. 2 are reported the XRD patterns of the lithium cobalt nitrides synthesized as a function of the cobalt content x in $Li_{3-2x}Co_xN$. It appears that the main diffraction lines of the parent nitride are maintained. This indicates the layered structure of Li_3N is not deeply modified which is consistent with a substitution of some interlayer lithium ions by cobalt ions. Two enlarged views of the XRD patterns are shown in the 15–40 and 40–90 2θ domains (Fig. 3). The increase in the Co content induces a significant shift of the 0 0 2, 1 0 1, 1 0 2 and 1 1 2 lines towards larger angle values, i.e., a decrease of the interlayer unit cell parameter c. In the same time, a shift of the 1 0 0, 1 1 0 and 2 0 0 diffraction peaks towards lower angle values corresponds to an increase of the a parameter. A more complicated behaviour is observed for the 0 0 1 line which vanishes for $x > 0.18$ and appears again for $R = 0.7$ (Fig. 3a). We will come back later on this specific point. For $R = 0.7$ and 0.8, typical lines of the lithium cobalt nitride $Li_{2.12}Co_{0.44}N$ are observed but the extraline at 44° (Fig. 3b) indicates a mixture of nitride and metallic cobalt showing that the maximum solubility of Co in Li_3N is achieved for $x = 0.44$. This limit is slightly higher than that suggested by Nishijima et al. [20,21] with a value of 0.4.

Assuming the structure of the lithium cobalt nitrides is very close to that of the initial structure of Li_3N as indicated by XRD patterns of Figs. 2 and 3, two structural models concerning the substitution of lithium ions by cobalt ions can be proposed: lithium ions in the Li_2N^- layers, i.e., in 2c sites (Wyckoff position: 2/3; 1/3; 0) or interlayer lithium ions located in the 1b sites (Wyckoff position: 0; 0; 1/2) can be substituted by Co ions. Table 2 summarizes the intensities of $h\,k\,l$ diffraction peaks calculated using a simulation for the XRD patterns for the two

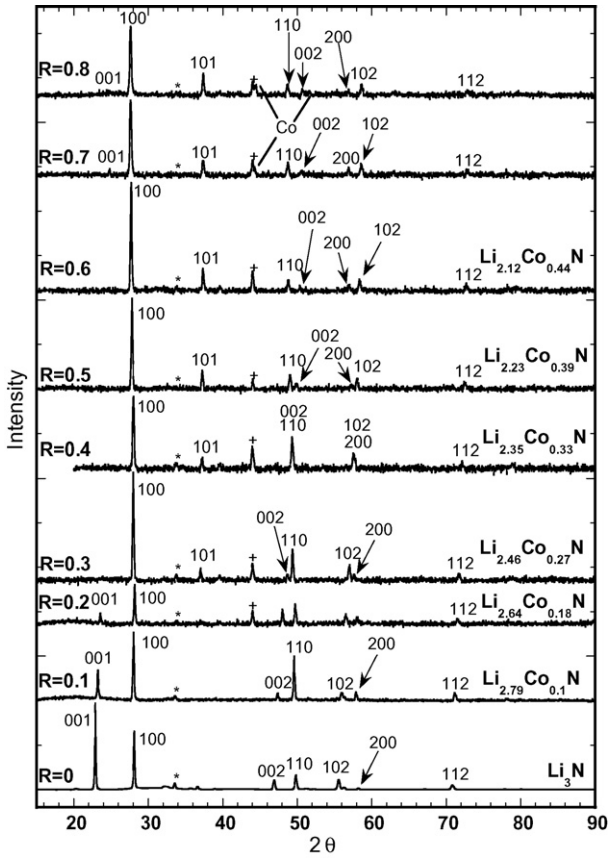

Fig. 2. X-ray diffraction patterns of the lithium cobalt nitrides $Li_{3-2x}Co_xN$ synthesized from a mixture of Co/Li_3N; R = the experimental molar ratio of reactants (Co/Li_3N), *: Li_2O, +: sample holder.

kinds of Co accommodation as a function of the Co content. The calculated data are compared with the values drawn from the experimental XRD diffraction patterns reported in Fig. 2.

As shown from this table, the main influence of the accommodation of cobalt ions instead of Li ions in 2c or 1b sites results in a great difference in the intensity of the 0 0 1, 1 0 0, 1 0 2 and 1 1 1 diffraction peaks. It is clear that the best fit is found for Co ions located in the interlayer sites (1b sites). In that case

Table 2
Influence of the Co distribution on the calculated intensities of diffraction lines as a function of the Co content x in $Li_{3-2x}Co_xN$ and comparison with the experimental data

($h\,k\,l$) reflection	0 0 1	1 0 0	1 0 1	0 0 2	1 1 0	1 0 2	1 1 1	2 0 0
Theoretical ratio I/I_{max} (%) (Co in 2c sites)								
$x = 0.18$	100	2	6	18	44	0	35	0
$x = 0.33$	100	1	13	17	40	1	37	0
$x = 0.44$	100	4	17	16	38	2	38	1
Theoretical ratio I/I_{max} (%) (Co in 1b sites)								
$x = 0.18$	9	100	9	18	41	18	2	7
$x = 0.33$	0	100	23	14	34	20	0	8
$x = 0.44$	1	100	31	13	31	20	1	8
Experimental ratio I/I_{max} (%)								
$x = 0.18$	40	100	26	36	49	43	9	28
$x = 0.33$	0	100	14	14	42	24	0	12
$x = 0.44$	6	100	25	9	21	22	7	16

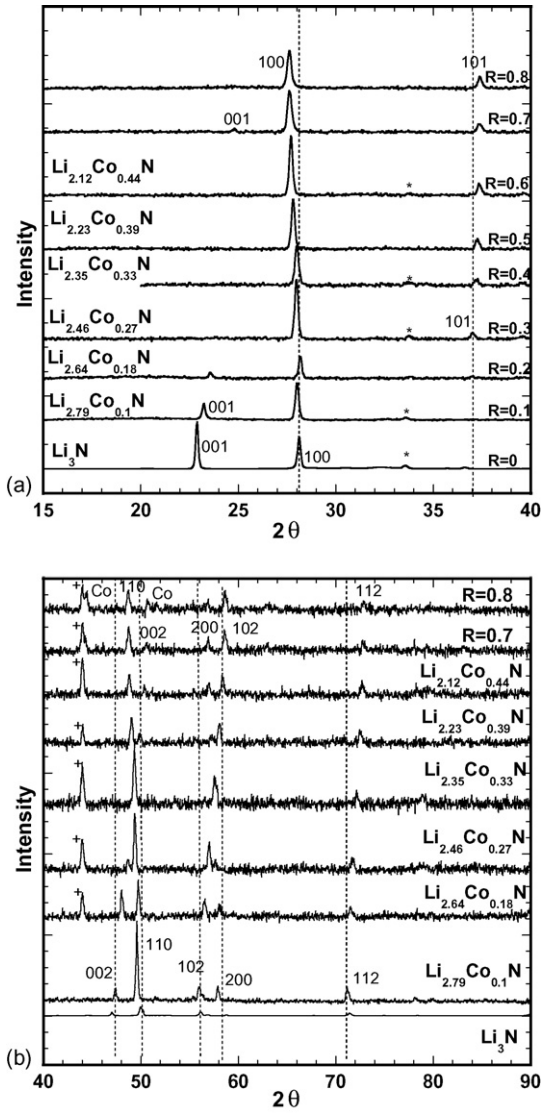

Fig. 3. Enlarged views of X-ray diffraction patterns of the lithium cobalt nitrides Li_{3-2x} Co_xN synthesized from a mixture of Co/Li_3N; (a) between 15° and 40° 2θ; (b) between 40° and 90° 2θ; R = the experimental molar ratio of reactants Co/Li_3N; *: Li_2O, +: sample holder.

the 1 0 0 peak is the strongest line, the 1 0 2 line exhibits a significant intensity while the 0 0 1, 1 1 1 diffraction lines are very weak or vanish. Hence, it can be inferred that the occupation of the cobalt ions take place in 1b sites whatever the cobalt content. This is in good accord with a previous assumption made for the $Li_{2.6}Co_{0.4}N$ compound [20].

Fig. 4 plots the variation of the cell parameters, a and c, as a function of the effective cobalt content per mole of ternary nitride. The lattice parameter a linearly increases with the cobalt content from 3.63(7) Å for $x = 0$–3.73(3) Å for $x = 0.44$ ($R = 0.6$). This trend can be explained by the larger ionic radius of Co^{2+} (<0.5 Å) [31] in comparison with that of Li^+. The correlative increase of the number of cation vacancies in the Li_2N^- sheet with the cobalt content is responsible for higher repulsive interactions beween N^{3-} ions in the ab plane. This effect could also explain the increase in the a parameter. A linear decrease is observed for the c parameter from 3.87(0) Å for $x = 0$ to reach

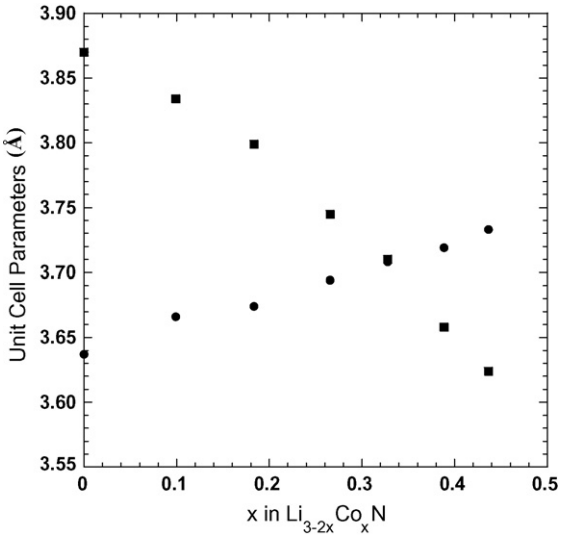

Fig. 4. Evolution of the unit cell parameters a (●) and c (■) as a function of x in $Li_{3-2x}Co_xN$.

3.62(4) Å for $x = 0.44$ ($R = 0.6$). The progressive substitution of Li^+ ions by more charged species, Co^{2+} ions, of similar size in the interlayer plane probably induces an enhancement of electrostatic attractive forces with the negatively charged Li_2N^- sheets. As a consequence of the lattice parameters variation, the $Li_{3-2x}Co_xN$ system exhibits a solid solution behaviour as illustrated by the linear decrease in the volume of the hexagonal unit cell versus the cobalt content. Even when linear evolutions of these unit cell parameters have been previously reported [20,26], some significant discrepancies appear. Indeed, in references [20,26] the Co content in the ternary nitride is assumed to exactly correspond to the initial amount of reactants used with a simple substitution reaction of Li^+ by Co^+ leading to the formula $Li_{3-x}Co_xN$. Moreover they reported a and c remain constant for $x = 0.5$ and 0.6 which can be explained by a Co content which does not exceed 0.44. The linear evolution of the cell volume versus Co content (Fig. 5) indicates a solid solution behaviour of the $Li_{3-2x}Co_xN$ system for $0.1 \leq x \leq 0.44$.

Fig. 6 shows the voltage profile of $Li_{3-2x}Co_xN$ electrodes discharged initially and then charged in the 0.02–1.0 V voltage range at $C/20$ rate. The second cycle is reported in order to avoid

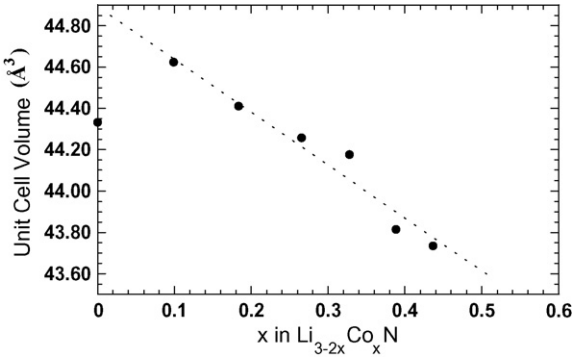

Fig. 5. Evolution of the unit cell volume of $Li_{3-2x}Co_xN$ vs. Co content (x) for $0.10 \leq x \leq 0.44$.

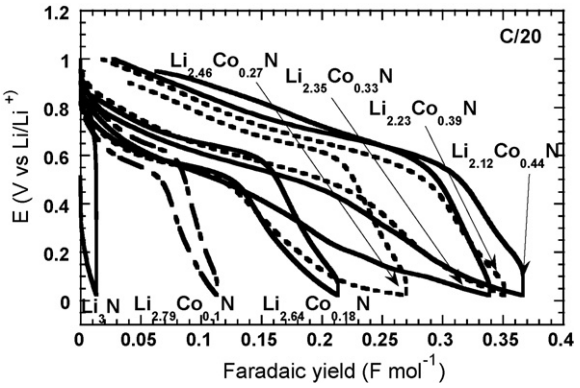

Fig. 6. Discharge–charge profiles of the $Li_{3-2x}Co_xN$ electrodes at *C*/20 in the 1/0.02 V potential range.

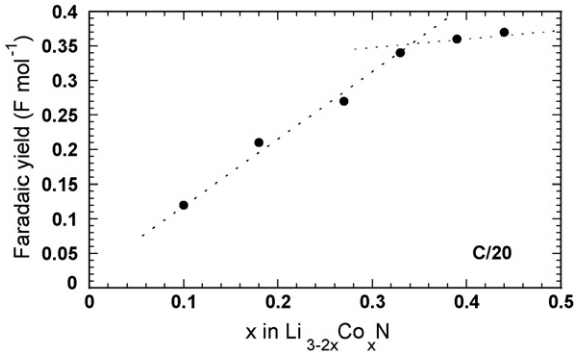

Fig. 7. Evolution of the faradaic yield vs. Co content *x* in $Li_{3-2x}Co_xN$.

the SEI formation to be included in the faradaic yield during the first reduction. We have checked that the pristine material Li_3N is not electroactive in this potential window. The discharge curve of lithium cobalt nitrides shows one main process located at 0.6 V with a lithium uptake which continuously increases with the cobalt content. The charge process is located near 0.7 V as a single signal and is practically quantitative. From Fig. 7 where the experimental lithium uptake obtained is reported as a linear function of the Co content, it can be seen that the Co ions are responsible for the reduction process. The electrochemical behaviour observed here is then well-consistent with the redox reaction of Co(II) into Co(I). For the Co-rich samples $Li_{2.23}Co_{0.39}N$ and $Li_{2.12}Co_{0.44}N$, the large Co content probably impedes to achieve the expected faradaic yield due to very strong repulsive interactions between interlayer Co^{2+} ions and Li^+ ions limiting then lithium diffusion in the material. Therefore the last two points in Fig. 7 deviate from the plot to reach lower values than that expected. It is surprising that the low Co contents $x = 0.1$ and 0.2 in $Li_{3-2x}Co_xN$ are reported in literature [21] to be inactive while the other compounds ($x = 0.3$; 0.4; 0.5) gave

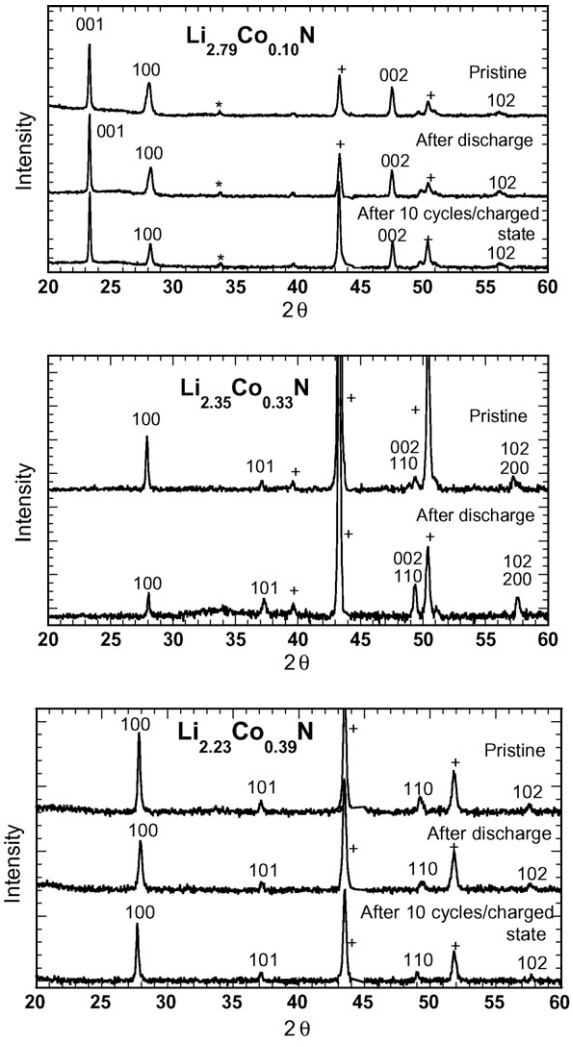

Fig. 8. X-ray diffraction patterns of the discharged and charged electrodes of: $Li_{2.79}Co_{0.10}N$, $Li_{2.35}Co_{0.33}N$ and $Li_{2.23}Co_{0.39}N$; *: Li_2O, +: sample support.

the same monotonous voltage profile and especially the same and low faradaic yield of 0.18 F mol^{-1} of nitride [21].

The XRD diffraction patterns of the fully discharged electrodes at 0.020 V and charged electrodes at 1 V are reported in Fig. 8 for three compounds: $Li_{2.79}Co_{0.10}N$, $Li_{2.35}Co_{0.33}N$ and $Li_{2.23}Co_{0.39}N$. In all cases, no significant change takes place except a negligible shift of some peaks which indicates that only a very slight variation of the lattice parameters occurs as Li insertion–extraction proceeds. The crystallinity of the host lattice is maintained and the values calculated for the unit cell parameters are summarized in Table 3. It comes out the change in the unit cell volume does not exceed 1% which is a very low value especially compared with the volumetric changes encountered in the Li–metal alloys. The absence of structural change

Table 3
Unit cell parameters of the discharged and charged electrodes of: $Li_{2.79}Co_{0.10}N$, $Li_{2.35}Co_{0.33}N$ and $Li_{2.23}Co_{0.39}N$

	$Li_{2.79}Co_{0.10}N$	$Li_{2.35}Co_{0.33}N$	$Li_{2.23}Co_{0.39}N$
After discharge at 0.02 V	$a = 3.65$ Å, $c = 3.82$ Å	$a = 3.68$ Å, $c = 3.69$ Å	$a = 3.71$ Å, $c = 3.67$ Å
After 10 cycles charged state	$a = 3.66$ Å, $c = 3.82$ Å		$a = 3.69$ Å, $c = 3.69$ Å

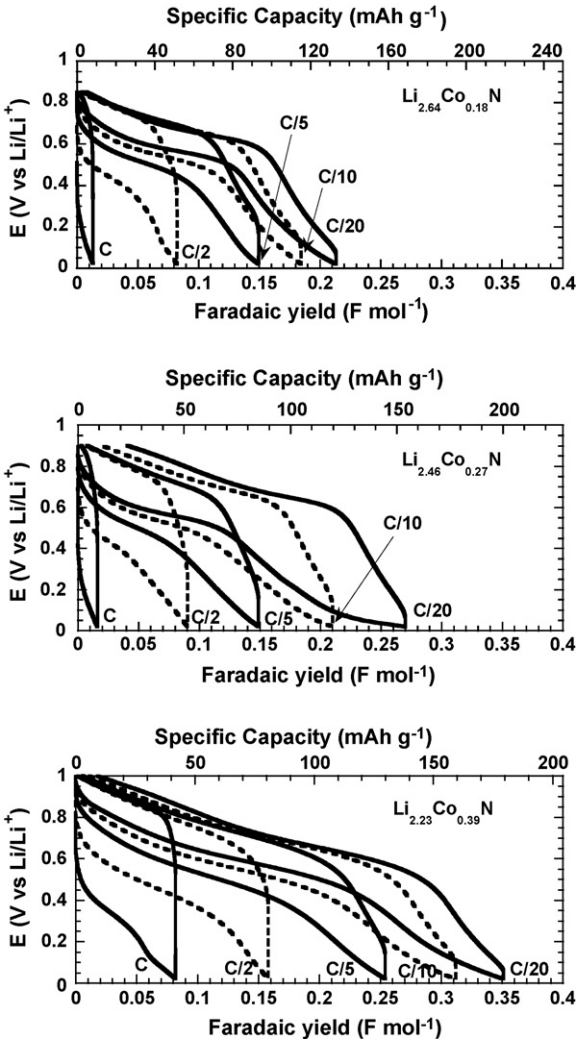

Fig. 9. Influence of the current density on the discharge–charge cycles of $Li_{2.64}Co_{0.18}N$, $Li_{2.46}Co_{0.27}N$ and $Li_{2.23}Co_{0.39}N$.

is consistent with the lithium accommodation occurring in the available cationic vacancies located in 2c sites of the Li_2N^- layer. Both the structural and the electrochemical experiments demonstrate the reduction of Co^{2+} into Co^+ accompanied by the Li insertion process in the lithium cobalt nitrides is reversible in the 0.02/1 V potential range following the equation:

$$[Li_{1-x}Co_x]_{1b}[Li_{2-x}[]_x]_{2c}N + zLi^+ + ze^- \overset{\text{reduction/oxidation}}{\longleftrightarrow} [Li_{1-x}Co_x]_{1b}[Li_{2-x+z}[]_{x-z}]_{2c}N$$

with $0 < x \leq 0.44$ and $z \leq x$.

This point is rarely addressed in literature but some contradictory data can be found on the redox species involved in the discharge mechanism: an electron energy loss spectroscopy study reports the presence of Co(I) in the pristine material $Li_{2.6}Co_{0.4}N$ [27] while an investigation using the EXAFS technique indicates that Li accommodation in the same compound takes place in vacant sites without giving evidence for the oxidation state of Co after reduction [32].

In Fig. 9 is illustrated the influence of the current density on the discharge–charge curves for three samples

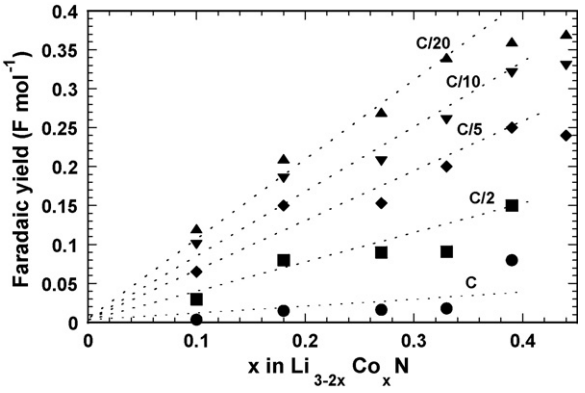

Fig. 10. Evolution of the faradaic yield as a function of Co content x in $Li_{3-2x}Co_xN$ and of the C rate.

$Li_{2.64}Co_{0.18}N$, $Li_{2.46}Co_{0.27}N$ and $Li_{2.23}Co_{0.39}N$. The faradaic yield strongly decreases with the current density for instance from 0.35 F mol^{-1} (i.e., 180 mAh g^{-1}) at C/20 to 0.08 F mol^{-1} (i.e., 40 mAh g^{-1}) at C rate in the case of $Li_{2.23}Co_{0.39}N$. A very close capacity is reported in [18] for $Li_{2.6}Co_{0.4}N$ but its chemical composition was not determined and the galvanostatic curves are not given hindering any comparison. As a general trend, it can be seen that these materials are highly sensitive to the current density since the capacity obtained at C/2 rate is only half the capacity achieved at C/10. However, it must be outlined that a quantitative charge process is systematically achieved showing the good rechargeability of these nitrides whatever the C rate. Even when the discharge curves are polarized from the C/5 rate, it is surprising to note that the charge curves do not exhibit such a drawback since the mean oxidation voltage always remains located at about 0.7 V.

Fig. 10 shows the faradaic yield increases linearly with the cobalt content whatever the C rate but reaches significant values only for C rates of C/5, C/10 and C/20 and cobalt content higher than 0.3. Owing to the low molar weight of these nitrides, a C/5 rate already corresponds to high current densities in the order of 100 mA g^{-1}.

The cycling properties of these lithium cobalt nitrides are then investigated as a function of the C rate in the 0.02 V/1 V (Fig. 11). The results expressed in terms of faradaic yield and specific capacity versus cycles, clearly indicate an excellent capacity retention whatever the rate. The higher value reported for the first discharge can be explained by the formation of the SEI in addition to the specific capacity expected for the active material. An interesting figure of merit of these materials is their ability to sustain high C rate without damaging the structure since the maximum capacity is recovered after a lower current density is applied. All these data characterizing a high reversible behaviour of the redox process are well consistent with the presence of a genuine Li intercalation reaction in the host lattice of lithium cobalt nitrides occurring without any structural change. For the best composition $Li_{2.23}Co_{0.39}N$, a stable specific capacity of 180 mAh g^{-1} is reached at C/20 and 140 mAh g^{-1} at C/5 over 50 cycles. This behaviour competes very well with TiO_2-based negative electrodes like $Li_4Ti_5O_{12}$ [33–36] sustaining higher C rate but

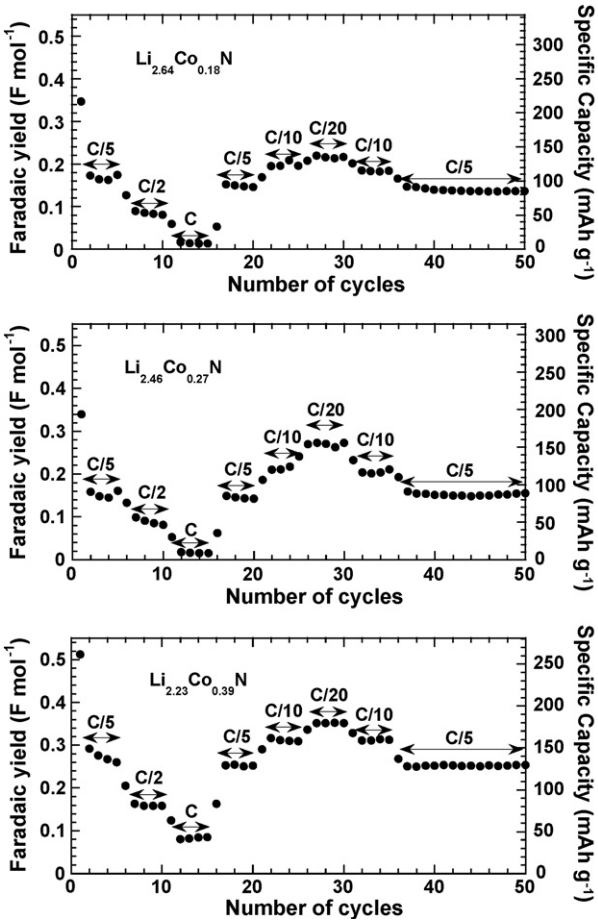

Fig. 11. Evolution of the faradaic yield and the specific capacity with galvanostatic cycles and *C* rate.

working at higher voltage, around 1.5 V against 0.6 V for these nitrides

This is confirmed by the XRD pattern of the $Li_{2.23}Co_{0.39}N$ electrode in the charged state after 10 cycles at *C*/5 (Fig. 8 and

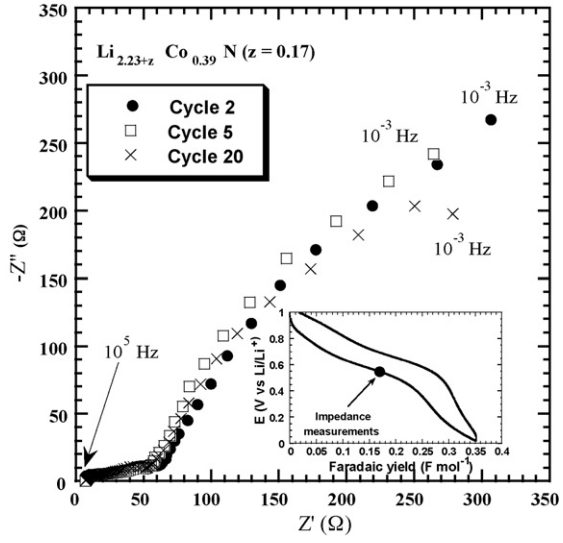

Fig. 12. ac impedance diagrams for $Li_{2.23+z}Co_{0.39}N$ at mid-discharge of cycles 2, 5 and 20 at *C*/5 rate. ($z = 0.17$).

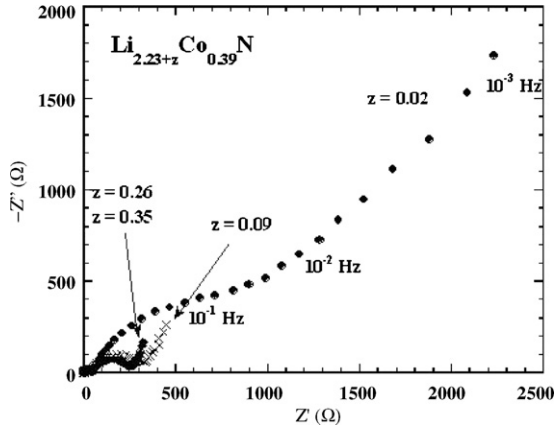

Fig. 13. ac impedance diagrams for $Li_{2.23}Co_{0.39}N$ as a function of the lithium uptake z in $Li_{2.23+z}Co_{0.39}N$.

Table 3). The main diffraction lines 1 0 0, 1 0 1, 1 1 0 and 1 0 2 of the pristine material are recovered at the same position showing no structural change occurs as Li intercalation proceeds.

ac impedance diagrams have been recorded at the mid-point of the discharge process for the $Li_{2.23+z}Co_{0.39}N$ compound ($z = 0.17$) for cycles 2, 5 and 20 (Fig. 12) with a stable capacity of 130 mAh g^{-1}. The diagrams practically superimpose in all the frequency range showing there is no change in the electrode surface area and no polarisation phenomenon which is in good accord with the stability of the capacity (Fig. 11) and the structure upon cycling (Fig. 8).

We have also examined the influence of the lithium uptake on the impedance diagrams. These experiments have been performed using Ni metal powder as conductive agent instead of acetylene black in order to minimize the SEI formation. The experimental data obtained for $Li_{2.23+z}Co_{0.39}N$ with $z = 0.02$, 0.09, 0.26, 0.35 are reported in Fig. 13. There is a strong discrepancy in the order of magnitude of the electrode impedance for $z = 0.02$ and higher lithium contents, i.e., for $z = 0.09$, 0.26 and 0.35. Indeed, the impedance rapidly decreases from 2270 Ω for $x = 0.02$ to 520 Ω for $z = 0.09$ and to 340 Ω for $z = 0.26$ and 0.35. A more detailed view of the high frequency and medium frequency regions is allowed in Fig. 14. This decrease in the impedance is explained by the strong decrease of the second semi-circle located at 0.245 Hz as soon as more than 0.02 Li ions are accommodated in the host lattice of the lithium cobalt

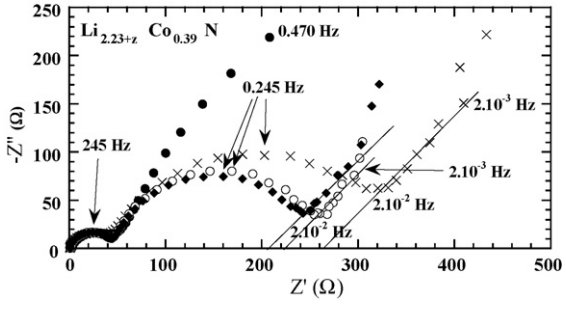

Fig. 14. Enlarged view of the high and medium frequency ranges of ac impedance diagrams for $Li_{2.23}Co_{0.39}N$ as a function of the lithium uptake z in $Li_{2.23+z}Co_{0.39}N$.

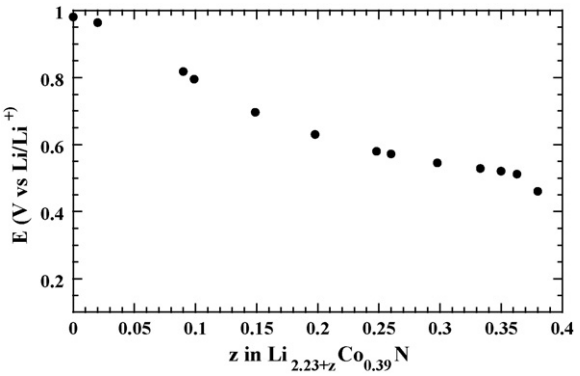

Fig. 15. OCV curve for $Li_{2.23+z}Co_{0.39}N$ at room temperature using pure Ni metal powder as conductive agent.

nitrides. Indeed, when $z > 0.02$, the second semi-circles superimpose and are characterized by the same characteristic frequency. Therefore, even when a better understanding of such signals is required to clearly ascribe the meaning of the two semi-circles, it is thought the second one located at 0.245 Hz is probably related with the charge transfer kinetics of the intercalation reaction ($j_0 \approx 10^{-4}$ A cm^{-2}). Indeed, the characteristic frequency (245 Hz) of the first semi-circle has also been observed for an electrode made of pure Ni powder. The sharp decrease in the charge transfer resistance for $x > 0.02$ could be explained by the improvement of the electronic conductivity properties due to an increase in the ratio of the mixed valencies Co^+/Co^{2+} for as lithium insertion proceeds. However the consumption of a passivating layer cannot be completely discarded to explain the sharp decrease of the impedance with the depth of discharge. In all cases, the second semi-circle is followed at medium and low frequencies (2×10^{-2} to 2×10^{-3} Hz) by a straight line with a phase angle of 45° from the real axis corresponding to the Warburg impedance and a capacitive line at low frequency ($f < 2 \times 10^{-3}$ Hz).

The apparent chemical diffusion coefficient D_{Li} can be calculated using the following equation when $\omega = 2\pi f \gg 2D_{Li}/L^2$:

$$D_{Li} = \left[\frac{V_M(dE/dx)_x}{F\sqrt{2}AS}\right]^2 \quad (1)$$

where A is obtained from the Warburg impedance ($Z_w = A\omega^{-1/2}$), V_M the molar volume of the compound (=26.38 cm^3 mol^{-1}), S the apparent surface area of the electrode, i.e., 2 cm^2 and $(dE/dx)_x$ is the slope, at fixed x, of the equilibrium potential composition curve (Fig. 15). L is the maximum length of the diffusion pathway (cm). The Warburg's region (2×10^{-2} to 2×10^{-3} Hz) corresponds to a frequency range where the kinetics of the system is almost entirely limited by the rate of the chemical diffusional process in the host material under semi-infinite conditions. The D_{Li} values are 2×10^{-10} cm^2 s^{-1} for $z = 0.09$; 0.26 and 8×10^{-11} cm^2 s^{-1} for $z = 0.36$. This slight decrease can be understood due to increasing repulsive interactions between Li ions in the layered host structure. Very few data are available on the Li diffusion kinetics in nitrides but the order of magnitude of these values compare well with that reported for the cubic phase $Li_{7-x}MnN_4$ [24].

4. Conclusion

We have shown that ternary nitrides in the Li–Co–N system can be synthesized from a Co/Li_3N mixture at 700 °C under a nitrogen flow with a cobalt and lithium loss during reaction. The as prepared phases correspond to the following chemical compositions: $Li_{2.79}Co_{0.10}N$, $Li_{2.64}Co_{0.18}N$, $Li_{2.46}Co_{0.27}N$, $Li_{2.35}Co_{0.33}N$, $Li_{2.23}Co_{0.39}N$, $Li_{2.12}Co_{0.44}N$. A simulation of the XRD patterns indicates that cobalt ions substitute for some Li ions in 1b site between Li_2N^- layers. The lithium cobalt nitrides exhibit a single step around 0.6 V in their discharge–charge profile obtained in the 1/0.02 V potential range and their capacity is found to be linearly dependent on the Co content. The structural and electrochemical behaviour reported here demonstrate that lithium/$Li_{3-2x}Co_xN$ cells operate by an intercalation mechanism of Li ions into cation vacancies (2c sites) involving reduction of Co^{2+} (1b site) into Co^+. Whatever the current density, stable specific capacities upon cycling are obtained due to the high stability of the layered structure and a value of 180 mAh g^{-1} at *C*/20 and 130 mAh g^{-1} at *C*/5 rate (100 mA cm^{-2}) is achieved for $Li_{2.23}Co_{0.39}N$. This work depicts for the first time a Li intercalation process involving a transition metal nitride while such a reaction is usually reported for many transition metal oxides.

Acknowledgement

The authors are indebted to the Centre National d'Etudes Spatiales (CNES) for financial support.

References

[1] M. Wakihara, Mater. Sci. Eng. R 33 (2001) 109.
[2] S. Flandrois, B. Simon, Carbon 37 (1999) 165.
[3] R. Yazami, Electrochim. Acta 45 (1999) 87.
[4] Y. Hamon, Y. Brousse, F. Jousse, P. Topart, P. Buvat, D.M. Schleich, J. Power Sources 96 (2001) 185.
[5] R.A. Huggins, J. Power Sources 81 (1999) 165.
[6] L. Rom, M. Wachtler, I. Papst, M. Schmied, J.O. Besenhard, F. Hofer, M. Winter, Solid State Ionics 143 (2001) 329.
[7] Y. Idota, T. Kubota, A. Matsufuji, T. Miyasaki, Science 276 (1997) 1394.
[8] I.A. Courtney, J.R. Dahn, J. Electrochem. Soc. 144 (1997) 2045.
[9] I.A. Courtney, J.R. Dahn, J. Electrochem. Soc. 144 (1997) 29.
[10] R.A. Huggins, Solid State Ionics 113–115 (1998) 57.
[11] P. Poizot, S. Laruelle, S. Grugeon, L. Dupont, J.-M. Tarascon, J. Power Sources 97–98 (2001) 235.
[12] J.-M. Tarascon, S. Grugeon, M. Morcrette, S. Laruelle, P. Rozier, P. Poizot, CR Chimie 8 (2005) 9.
[13] F. Gillot, M.P. Bichat, F. Favier, M. Morcrette, M.L. Doublet, L. Monconduit, Electrochim. Acta 49 (2004) 2325.
[14] M.P. Bichat, T. Politova, J.L. Pascal, F. Favier, L. Monconduit, J. Electrochem. Soc. 151 (2004) A2074.
[15] F. Gillot, L. Moncounduit, M.L. Doublet, Chem. Mater. 17 (2005) 5817.
[16] S. Boyanov, J. Bernardi, F. Gillot, L. Dupont, M. Womes, J.M. Tarascon, L. Monconduit, M.L. Doublet, Chem. Mater. 18 (2006) 3531.
[17] L.M.L. Fransson, J.T. Vaughey, R. Benedek, K. Edström, J.O. Thomas, M.M. Thackeray, Electrochem. Commun. 3 (2001) 317.
[18] T. Shodai, S. Okada, S. Tobishima, J. Yamaki, Solid State Ionics 86–88 (1996) 785.
[19] T. Shodai, S. Okada, S. Tobishima, J. Yamaki, J. Power Sources 68 (1997) 515.
[20] M. Nishijima, T. Kagohashi, N. Imanishi, Y. Takeda, O. Yamamoto, S. Kondo, Solid State Ionics 83 (1996) 107.

[21] M. Nishijima, T. Kagohashi, Y. Takeda, M. Imanishi, O. Yamamoto, J. Power Sources 68 (1997) 510.
[22] T. Shodai, Y. Sakurai, T. Suzuki, Solid State Ionics 122 (1999) 85.
[23] J.L.C. Rowsell, V. Pralong, L.F. Nazar, J. Am. Chem. Soc. 123 (2001) 8598.
[24] M. Nishijima, Y. Takeda, N. Imanishi, O. Yamamoto, J. Solid State Chem. 113 (1994) 205.
[25] M. Nishijima, N. Tadokoro, Y. Takeda, N. Imanishi, O. Yamamoto, J. Electrochem. Soc. 141 (1994) 2966.
[26] W. Sachsze, R. Juza, Z. Anorg. Chem. 259 (1949) 278.
[27] S. Suzuki, T. Shodai, J. Yamaki, J. Phys. Chem. Solids 59 (1998) 331.
[28] J. Yang, Y. Takeda, N. Imanishi, O. Yamamoto, J. Electrochem. Soc. 147 (2000) 1671.
[29] J. Klatyk, W. Schnelle, F.R. Wagner, R. Niewa, P. Novák, R. Kniep, M. Waldeck, V. Ksenofontov, P. Gütlich, Phys. Rev. Lett. 88 (2002) 1.
[30] Y. Takeda, M. Nishijima, M. Yamahata, K. Takeda, N. Imanishi, O. Yamamoto, Solid State Ionics 130 (2000) 61.
[31] W.H. Baur, Cryst. Rev. 1 (1987) 59.
[32] T.Y. Kim, M.G. Kim, J.M. Lee, T. Kang, H.J. Sohn, Electrochem. Solid State Lett. 5 (2002) A103.
[33] E. Ferg, R.J. Gummow, A. de Kock, J. Electrochem. Soc. 141 (1994) L147.
[34] K.M. Colbow, J.R. Dahn, R.R. Haering, J. Power Sources 26 (1989) 397.
[35] T. Ohzuku, A. Ueda, N. Yamamoto, J. Electrochem. Soc. 142 (1995) 1431.
[36] T. Ohzuku, A. Ueda, N. Yamamoto, Y. Iwakoshi, J. Power Sources 54 (1995) 99.